Photochemical & Photobiological Sciences (2022) 21:1677–1687
https://doi.org/10.1007/s43630-022-00250-y

ORIGINAL PAPERS

Phototoxicity of BODIPY in long-term imaging can be reduced by intramolecular motion

Iida Kähärä[1] · Nikita Durandin[1] · Polina Ilina[2] · Alexander Efimov[1] · Timo Laaksonen[1,2] · Elina Vuorimaa-Laukkanen[1] · Ekaterina Lisitsyna[1]

Received: 14 December 2021 / Accepted: 23 May 2022 / Published online: 7 July 2022

Abstract

For long-term live-cell fluorescence imaging and biosensing, it is crucial to work with a dye that has high fluorescence quantum yield and photostability without being detrimental to the cells. In this paper, we demonstrate that neutral boron-dipyrromethene (BODIPY)-based molecular rotors have great properties for high-light-dosage demanding live-cell fluorescence imaging applications that require repetitive illuminations. In molecular rotors, an intramolecular rotation (IMR) allows an alternative route for the decay of the singlet excited state (S_1) via the formation of an intramolecular charge transfer state (CT). The occurrence of IMR reduces the probability of the formation of a triplet state (T_1) which could further react with molecular oxygen ($^3O_2$) to form cytotoxic reactive oxygen species, e.g., singlet oxygen ($^1O_2$). We demonstrate that the oxygen-related nature of the phototoxicity for BODIPY derivatives can be significantly reduced if a neutral molecular rotor is used as a probe. The studied neutral molecular rotor probe shows remarkably lower phototoxicity when compared with both the non-rotating BODIPY derivative and the cationic BODIPY-based molecular rotor in different light dosages and dye concentrations. It is also evident that the charge and localization of the fluorescent probe are as significant as the IMR in terms of the phototoxicity in a long-term live-cell imaging.

Graphical abstract

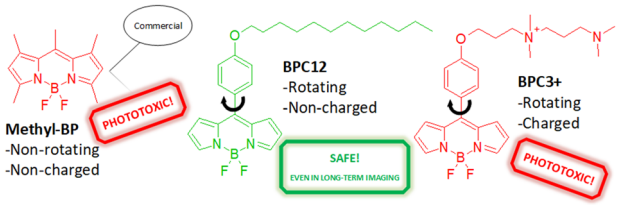

Keywords Boron-dipyrromethene (BODIPY) · Intramolecular rotation (IMR) · Phototoxicity · Singlet oxygen · Viability assay

✉ Iida Kähärä
iida.kahara@tuni.fi

✉ Ekaterina Lisitsyna
ekaterina.lisitsyna@tuni.fi

[1] Chemistry and Advanced Materials, Unit of Materials Science and Environmental Engineering, Faculty of Engineering and Natural Sciences, Tampere University, P.O. Box 541, 33014 Tampere, Finland

[2] Division of Pharmaceutical Biosciences, Faculty of Pharmacy, University of Helsinki, P.O. Box 56, 00014 Helsinki, Finland

1 Introduction

In live-cell fluorescence microscopy, boron-dipyrromethene (BODIPY) derivatives are commonly used to tag proteins and lipophilic cellular structures due to their high extinction coefficients, fluorescence quantum yields and photostability [1]. Recently, BODIPY molecules have been tailored to work as molecular rotors by introducing a phenyl-substituent in the meso-position of the BODIPY core structure [2]. Upon photoexcitation, the BODIPY-based molecular rotors

can undergo an intramolecular rotation (IMR, Fig. 1), where the twisted conformation with the phenyl ring having a dihedral angle of 55° turns into a planar structure of 0° or 180° [3]. Upon rotation of the phenyl ring, a charge transfer from the BODIPY core to the phenyl-substituent takes place. The formed charge transfer (CT, Fig. 1) state relaxes via an internal conversion (IC^{CT}, Fig. 1) to the ground electronic state, thus reducing the probability of fluorescence and intersystem crossing (ISC^{S}, Fig. 1). This relaxation pathway for BODIPY-based molecular rotors has been proven by Kee et al. [4], Prlj et al. [5] and Polita et al. [6] by time-dependent density functional theory (TD-DFT) calculations. The probability of IMR strongly depends on the micro-environment of the dye (e.g., solvent viscosity and polarity [7]). Consequently, BODIPY-based molecular rotors are an excellent choice for measuring intracellular temperature [8] and viscosity [9–12], for the characterization of a polymer self-assembly [13], as apoptosis markers [14] and as selective ion [15] or gas [16] sensors.

On the other hand, the BODIPY derivatives can be quite phototoxic that is especially disadvantageous in long-term live-cell imaging. Dyes in general may undergo an intersystem-crossing (ISC^{S}, Fig. 1) leading to a formation of the triplet state (T_1, Fig. 1). Before the triplet state decaying via phosphorescence and/or internal conversion (IC^{T}, Fig. 1), it may react with molecular oxygen ($^3O_2$, Fig. 1) to form reactive oxygen species including singlet oxygen ($^1O_2$, Fig. 1) [17]. Singlet oxygen is known to cause an oxidative stress and as a result cell death [18]. This phenomenon is absent or negligible in short-term imaging (having single or several

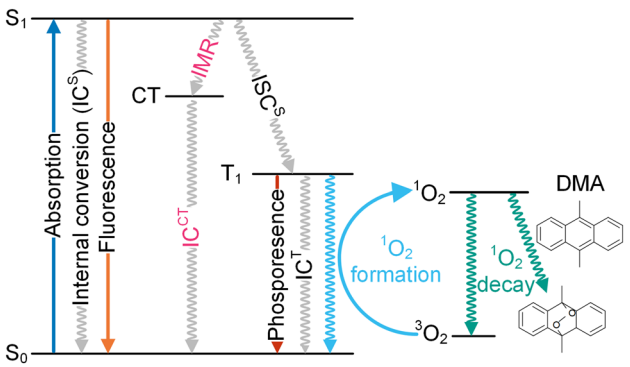

Fig. 1 Photophysical processes of molecular rotors including an intramolecular rotation (IMR) process, which leads to a formation of charge transfer (CT) state with a subsequent internal conversion (IC) accompanied by charge recombination. For a molecule without or with a restricted intramolecular rotation, in addition to fluorescence and IC^{S}, a direct ISC^{S} from singlet excited state can take place. Singlet oxygen ($^1O_2$) formation and decay processes (light blue) and the reaction of dimethyl anthracene (DMA) with singlet oxygen to form endoperoxide compound (green) are also indicated. Straight lines represent radiative processes and wavy lines nonradiative ones. Pink text designates more probable processes for rotor molecules

illuminations) but may become critical in longer imaging experiments. For example, in fluorescence lifetime imaging microscopy [19] and two-photon laser scanning microscopy [20] the non-phototoxicity of the dye becomes a very essential requirement when performing experiments lasting up to 24 h. Moreover, multiple illuminations in the long-term imaging may lead to a light exposure comparable to the high-light-dose imaging, e.g., super-resolution microscopy, where the strategies of reducing phototoxicity have recently gained attention [21].

In this study, we demonstrate that the BODIPY-based molecular rotors, which allow IMR, show significantly lower phototoxicity than a non-rotor BODIPY derivative. For the molecular rotors, the intramolecular rotation (IMR, $S_1 \rightarrow CT$, Fig. 1) offers an additional relaxation route that competes with fluorescence and intersystem-crossing (ISC^{S}, $S_1 \rightarrow T_1$, Fig. 1) processes. According to Kee et al. [4], there is virtually no barrier to rotation of the phenyl group toward planarity. The formed CT state has efficient coupling to the ground state via nonradiative processes making the IMR process more favorable than fluorescence or ISC^{S}. Thus, the triplet state formation and, consequently, the singlet oxygen generation are reduced. It also explains the low fluorescence quantum yields observed for rotor-BODIPYs.

Two BODIPY-based molecular rotors, BPC12 and BPC3+ (Chart 1A) studied here have been previously used to map intracellular viscosities with fluorescence lifetime imaging microscopy [12, 22, 23]. They are compared in solution and living cell studies with a commercial non-rotor dye, Methyl-BP (Chart 1A) which is commonly used to stain oils, polymers and neutral lipids e.g., lipid droplets [24, 25]. The Methyl-BP cannot form a charge transfer (CT, Fig. 1) state, and therefore, it has one relaxation route less to compete with ISC^{S} to triplet state ($S_1 \rightarrow T_1$, Fig. 1).

In the present work, the absorption and fluorescence maxima, the Stokes shifts, the fluorescence quantum yields, and the normalized singlet oxygen quantum yields of all the three BODIPY derivatives are compared in the solvents of different polarity. The effects of the dye concentration, the light dosage and the presence of oxygen are explored by fluorescence microscopy and cell viability studies with a human prostate cancer cell line (PC-3) as an example. Cellular localization of the dyes is studied by co-localization experiments with a mitochondrial marker in HeLa adenocarcinoma cell line (ATCC CCL-2).

2 Experimental section

2.1 Dyes, reagents, and solvents

Solvents and compounds were used as obtained if not otherwise mentioned. Toluene and dichloromethane (DCM)

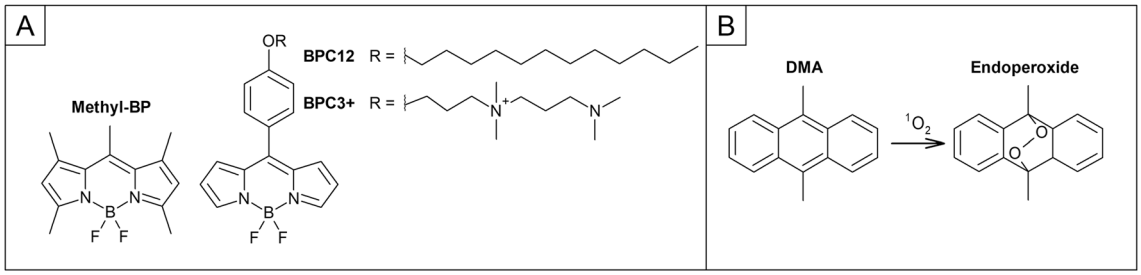

Chart 1 Molecular structures of **A** the BODIPY derivatives; Methyl-BP, BPC12 and BPC3+. **B** Reaction of the DMA with a singlet oxygen ($^1O_2$) to form the endoperoxide compound

was acquired from VWR International Oy (Wayne, Pennsylvania, USA). Ethanol (EtOH) was purchased from Altia Industrial (Helsinki, Finland). Dimethyl sulfoxide (DMSO), difluoro{2–1-(3,5-dimethyl-2H-pyrrol-2-ylidene-N)ethyl-3,5-dimethyl-1H-pyrrolato-N}boron (Methyl-BP, Cat. No. D3922, Invitrogen BODIPY 493/503, Chart 1A) and 9,10-dimethylanthracene (DMA, Chart 1B) were purchased from Sigma-Aldrich (Merck KGaA, Darmstadt, Germany). BPC12 (Chart 1A) was synthesized according to the procedure described in Wagner and Lindsey [26]. BPC3+ (Chart 1A) was kindly provided by Dr. Marina Kuimova (Imperial College London), and synthesized in her laboratories according to the procedure described in the Supporting Information of Sherin et al. [23]

2.2 Absorption and fluorescence spectroscopy

An UVPC-3600 spectrophotometer (Shimadzu, Kyoto, Japan) was used to record absorption spectra. Fluorescence spectra were measured with a Fluorolog®-3 spectrofluorometer (Horiba, Minami-ku Kyoto, Japan). An FLS-1000 spectrofluorometer (Edinburg Instruments, Livingston, UK) was used as an excitation source to generate 500 nm light in the experiments of Sect. 2.4.

2.3 Determination of relative fluorescence quantum yields

Fluorescence quantum yields (Φ_{fl}, Eq. 1) were determined for the Methyl-BP, BPC12 and BPC3+ dyes in EtOH, DMSO and toluene using the Methyl-BP in EtOH as a reference with a known fluorescence quantum yield ($\Phi_{fl,ref}$, Eq. 1) of 85% [27]:

$$\Phi_{fl} = \Phi_{fl,ref}\left(A_{ref}/A\right)\left(I/I_{ref}\right)\left(n/n_{ref}\right)^2 \quad (1)$$

where A and A_{ref} are the absorbances at 500 nm (excitation wavelength), I and I_{ref} are the integrals of the monitored fluorescence spectra, and n and n_{ref} are the refractive indices of the used solvents (Table S1) for the studied samples and the reference, respectively. Absorbances of the samples at 500 nm were ≈ 0.13 when recording the absorption and fluorescence spectra.

2.4 Indirect detection of singlet oxygen

Normalized singlet oxygen quantum yields were defined using an indirect method with the help of DMA as a singlet oxygen sensor. DMA can form an endoperoxide compound (Chart 1B) upon interaction with singlet oxygen, which results in a pronounced decrease in its absorption spectrum.

Briefly, 20 µM solutions of the three studied BODIPY derivatives (Chart 1A) were prepared in toluene and DMSO, and further supplemented with 200 µM DMA. The samples were illuminated with 500 nm light followed by recording of their absorption spectra at different exposure times. For each time point and sample, the area under the DMA absorption was calculated by integrating, and it was further normalized to the zero time point of each sample. The normalized integrals of DMA absorption were first plotted against the illumination time and then fitted using an exponential decay function in Origin software (OriginLab, Massachusetts, USA) (Fig. S1) to obtain rate constants for the DMA endoperoxide formation (Chart 1B). The rate constants were used for calculating the singlet oxygen quantum yields (Φ_Δ) with Eq. (2):

$$\Phi_\Delta = An^2/k \quad (2)$$

where A is the absorbance at 500 nm, k is the rate constant of endoperoxide formation, and n is the refractive index of the used solvent (Table S1). The computed singlet oxygen quantum yields were further normalized against Methyl-BP in toluene to obtain normalized singlet oxygen quantum yields ($\Phi_{\Delta,norm}$).

2.5 Cell culturing and seeding

Gibco™ (ThermoFisher Scientific, Massachusetts, USA) reagents were used for cell culturing. Human prostate cancer

cell line (PC-3, ATCC, Virginia, USA) was maintained in Ham's F-12 K (Kaighn's) Medium with 10% (v/v) Fetal Bovine Serum (FBS), and 100 units/ml penicillin and streptomycin at + 37 °C and 5% CO_2.

One day before the illumination procedure 12 500 PC-3 cells per a well were seeded into a white, clear-bottom polystyrene microplate (96 Well Microplate, mClear, ®Chimney Well, Greiner Bio-One GmbH). FluoroBrite DMEM Medium supplemented with 10% (v/v) FBS and 100 units/ml penicillin and streptomycin was used as a complete growth medium during the illumination procedure and was renewed 24 h after the illumination procedure, to reduce a background fluorescence signal during a live-cell fluorescence imaging.

2.6 Illumination procedure in phototoxicity experiments

One hour before the illuminations, the growth medium was replaced with treatment solutions containing the Methyl-BP, BPC12 and BPC3+ dyes in FluoroBrite DMEM complete growth medium. The final concentrations of the BODIPY derivatives in the treatment solutions were 0.6 µM, 1.5 µM, 3.0 µM and 6.0 µM, whereas the DMSO content did not exceed 1% (v/v). The solution of DMSO 1% (v/v) in complete growth medium without any illumination (i.e., kept in the dark) was used as a 100% survival control. DMSO 1% (v/v) with 0.1% (v/v) Triton™ X-100 Surfact-Amps™ Detergent Solution (Thermo Scientific™, Massachusetts, USA) in complete growth medium was used as a positive control.

During the illumination procedure, the microplate was placed inside of a custom-made incubator with a constant flow of a 95% air and 5% CO_2 gas mixture at 37 °C for ensuring an optimal, normoxic (20.95% of oxygen) conditions for the cells. Hypoxic (≈ 0.08% of oxygen) conditions were created by replacing the air with a N_2 flow for 2 h prior to the illumination procedure. The oxygen level inside the incubator was measured using 1 channel fiber-optical meter FireSting-O_2 and oxygen sensor spots (Pyro Science, Aachen, Germany). One-point calibration (ambient air) has been performed before use following manufacturer's protocol.

For revealing the possible phototoxic effect of the dyes, one well at a time was illuminated with a 490 nm LED [M90L4, 205 mW (Min) Mounted LED, 350 mA, Thorlabs, Inc., Newton, New Jersey, USA] using 41 mW power at 4.75 cm distance from the bottom of the microplate. Other wells were protected from the light. The phototoxicity experiments were performed with three different light dosages of 13.4 J/cm^2, 26.8 J/cm^2, and 53.5 J/cm^2. These light dosages were obtained from LED's ≈ 27 mW/cm^2 power density by changing the illumination time to 8 min, 17 min or 33 min, respectively. At least 3 independent repeats of each illumination procedure were performed for every treatment. The illumination procedure was followed by a 24-h incubation in a cell incubator at + 37 °C and 5% CO_2.

2.7 Fluorescence imaging

24 h after the illumination procedure, fluorescence microscopy images were obtained using an Axio Observer fluorescence microscope (Zeiss, Oberkochen, Germany) equipped with a 20× air objective and a mercury short arc reflector lamp as a light source. A Filter Set 38 HE (Zeiss, Oberkochen, Germany) was used to provide an excitation wavelength of 470/40 nm and an emission wavelength of 525/50 nm.

2.8 Viability assays

CellTiter-Glo® Luminescent Cell Viability Assay (G7570, Promega Corporation, USA), which is based on the quantitation of the present ATP (an indicator of metabolically active cells), was performed 24 h after the illumination procedure, subsequent to the fluorescence microscopy, according to the protocol provided by the manufacturer [28]. Luminescence signal was recorded with a Chameleon multilabel microplate reader (Hidex, Turku, Finland) with the integration time of 1 s per well.

Luminescence intensities obtained from each treatment were computed into viability percentages normalized to 100% survival control [DMSO 1% (v/v) in the dark]. The triplicates of viability percentages obtained in the independent repeats of the same treatment were averaged and 95% confidence intervals were determined in Excel software (Microsoft Corporation, Redmond, Washington, USA). For calculating P-values of an independent T test, a built-in function of Excel software was used.

2.9 Co-localization

HeLa adenocarcinoma cell line (ATCC CCL-2) was kindly provided by Prof. Arto Urtti, University of Helsinki, Finland. The cells were maintained in RPMI 1640 medium (Gibco) with 10% FBS. One day before experiment, the cells were seeded to a black frame clear-bottom 96-well plates (Falcon), 10 000 cells/well. The staining solution was prepared in FluoroBrite DMEM by adding test dyes to a final concentration 6 µM, live-cell Mitotracker Deep Red 628/672 (Invitrogen M22426) to a final concentration 500 nm and Hoechst 33342 to 5 µg/ml. The growth medium in the wells was carefully replaced by 100 µL of the staining solution and the plate was incubated at 37 °C, 5% CO_2 for 90 min. After the incubation the cells were fixed by adding equal volume of 8% paraformaldehyde (PFA) for 20 min. Then

Table 1 Absorption maxima λ_{abs}, fluorescence maxima λ_{fl}, Stokes shifts $\Delta\lambda$ and fluorescence quantum yields Φ_{fl} of Methyl-BP, BPC12 and BPC3+ in EtOH, DMSO and toluene. Normalized singlet oxygen quantum yields $\Phi_{\Delta,norm}$ for Methyl-BP, BPC12 and BPC3+ in DMSO and toluene presented by mean ± standard deviation calculated from triplicates. Polarities of EtOH, DMSO and toluene

Solvent	Dye	λ_{abs} (nm)	λ_{fl} (nm)	$\Delta\lambda$ (nm)	Φ_{fl} (%)	$\Phi_{\Delta,norm}$	Polarity
EtOH	Methyl-BP	495	506	11	85 [27]	–	0.654 [29]
	BPC12	495	510	15	3.9	–	
	BPC3+	496	513	17	1.7	–	
DMSO	Methyl-BP	496	511	15	86.2	0.74 ± 0.03	0.444 [29]
	BPC12	498	517	19	4.5	0.36 ± 0.02	
	BPC3+	499	518	19	3.8	0.13 ± 0.05	
Toluene	Methyl-BP	500	512	12	96.8	1.00 ± 0.03	0.099 [29]
	BPC12	501	517	16	10.1	0.26 ± 0.02	
	BPC3+	502	518	16	2.3	1.13 ± 0.04	

cells were washed 3 times with HBSS and stored at + 4 °C until imaging. The imaging was performed using Cytation 5 imaging reader (BioTek) equipped with 20× Plan Fluorite phase-contrast NA 0.45 objective (Olympus 1,320,517) and filter cubes for DAPI to visualize Hoechst 33342, Cy5 to visualize Mitotracker and GFP to visualize test dyes.

3 Results and discussion

3.1 Spectroscopic characterization of BODIPY derivatives

The spectral properties of the Methyl-BP, BPC12 and BPC3+ dyes are clearly solvent-dependent. The maximum wavelength of absorption (λ_{abs}) and fluorescence (λ_{fl}) spectra, the Stokes shifts ($\Delta\lambda$), the fluorescence quantum yields (Φ_{fl}) for all the dyes, and the polarities of the used solvents are presented in Table 1. The absorption and fluorescence spectra of the dyes in EtOH, DMSO and toluene are given in Fig. S2 of the Supporting Information. In EtOH, the absorption and emission maxima are both the most blue-shifted for all the BODIPY derivatives, while in toluene the spectra are the most red-shifted, thus following the polarity change of the solvent (Table 1). The Stokes shifts for all the studied BODIPY derivatives are the largest in DMSO and the lowest in EtOH or toluene depending on the dye.

The Methyl-BP has clearly higher fluorescence quantum yields (85–96.8%, Table 1) compared with the BODIPY-based molecular rotors regardless the solvent. This is a logical result of the reduced possibility for the Methyl-BP excited state to relax via nonradiative pathways due to the absence of an intramolecular rotation [30]. The fluorescence quantum yield of Methyl-BP is the highest in toluene, and the quantum yield decreases as the polarity of the solvent increases.

In the rotor molecules, the intramolecular rotation (IMR) favors the nonradiative relaxation via the CT state over the direct singlet state relaxation to the ground state $S_1 \rightarrow S_0$ (Fig. 1), leading to the low fluorescence quantum yields (1.7–10.1%, Table 1) [9]. The BPC12 rotor has a polarity-dependent fluorescence quantum yield, like the Methyl-BP, decreasing from 10.1% in nonpolar toluene to 4.5% and 3.9% in polar DMSO and EtOH, respectively. However, the positively charged BPC3+ rotor has equally low fluorescence quantum yields in polar EtOH (1.7%) and in nonpolar toluene (2.3%) outlying the above concept. This is probably due to intermolecular interactions between the positively charged BPC3+ molecules in the nonpolar environment. The broadened absorption spectrum of the BPC3+ in toluene (Fig. S2, bottom graph) supports this explanation. Concentration-dependent absorption studies for the BPC3+ in toluene and dichloromethane (DCM) confirm the presence of intermolecular interactions between BPC3+ molecules in toluene (Supporting information, Fig. S3). In DCM no spectral changes are observed, while in toluene the spectrum broadens, and its maximum shifts to longer wavelengths as the concentration decreases.

3.2 Normalized quantum yields of singlet oxygen

In this study, singlet oxygen was detected using DMA as a singlet oxygen probe upon a selective excitation of the studied BODIPY derivatives in DMSO and toluene. The averaged integrals of DMA absorption plotted against the illumination time are presented in Fig. S1 of the Supporting Information. Using the indirect method, we aimed to reveal how the singlet oxygen quantum yield changes for the studied dyes in different solvents instead of measuring their absolute values. Thus, normalized values were used when the singlet oxygen quantum yield in the presence of Methyl-BP in toluene was set as 1.00. The final normalized singlet oxygen quantum yields ($\Phi_{\Delta,norm}$) are presented in Table 1. Since the singlet oxygen is formed in a reaction between the ground state oxygen and the triplet state of the dyes, the possible photochemical process leading to the dye triplet state formation, i.e., direct ISC^S from S_1 state ($S_1 \rightarrow T_1$, Fig. 1), must be considered. This process is competing with other relaxation processes: fluorescence,

internal conversion (IC^S) and IMR. It is important to note that the IMR is a polarity-dependent process [31–33].

Although, Methyl-BP has low possibility to form a triplet state due to the high fluorescence quantum yields (85–97%), the triplet state amount seems to be higher than that of the rotor dyes. The normalized singlet oxygen quantum yield in the presence of the Methyl-BP in DMSO is remarkably higher (0.74) than for either of the rotors (0.13–0.36). This is attributed to the absence of IMR in the rigid Methyl-BP molecule, thus allowing the ISC^S to the triplet state ($S_1 \rightarrow T_1$, Fig. 1). Therefore, it appears that the IMR competes more effectively with the ISC^S in the studied rotor dyes than the fluorescence does in the non-rotor derivate.

The singlet oxygen quantum yield of the Methyl-BP in toluene is slightly higher than in DMSO (1.00 and 0.74, respectively, Table 1), that can be explained by a difference in the polarities of the solvents (Table 1). Besides this, approximately 6 times higher oxygen solubility in toluene (9.23×10^4 mol fractions) compared with that in DMSO (1.57×10^4 mol fractions) may partly increase the possibility of singlet oxygen formation in toluene [34]. In addition, the ability of DMSO to react with singlet oxygen to form dimethyl sulfone [35], may reduce the singlet oxygen concentration in the studied samples. In contrast to the Methyl-BP, the molecular rotors undergo the IMR rather than the ISC^S, consequently leading to a reduced population of the rotors' triplet states and a consequent decrease of the singlet oxygen generation [9]. For the BPC12, the singlet oxygen quantum yields in DMSO and in toluene are nearly similar (0.36 vs. 0.26, correspondingly) suggesting that the behavior of BPC12 is independent of solvent polarity. Contrary to BPC12, the singlet oxygen quantum yield in the presence of the BPC3+ in toluene is surprisingly close or even slightly higher than the value for the Methyl-BP (1.13 vs. 1.00, respectively, Table 1). This behavior of the BPC3+ agrees with the unexpectedly low fluorescence quantum yield of the dye in toluene (2.3%, Table 1). Apparently, the difference in the chemical structure of the rotors results in their different behavior. It appears that the intermolecular interactions between positively charged BPC3+ molecules in toluene hamper the IMR process, hence facilitating the ISC^S process from a singlet excited state ($S_1 \rightarrow T_1$, Fig. 1). While the solvent polarity does not significantly influence the behavior of neutral BPC12.

3.3 Phototoxic effect

Since all the studied BODIPY derivatives generated singlet oxygen, which is harmful for cells [18], the phototoxic effect of each studied BODIPY derivative towards the PC-3 cells was determined. Therefore, cell morphology changes and viabilities in the presence of the BODIPY derivatives were tracked at different dye concentrations, light dosages, and oxygen concentrations.

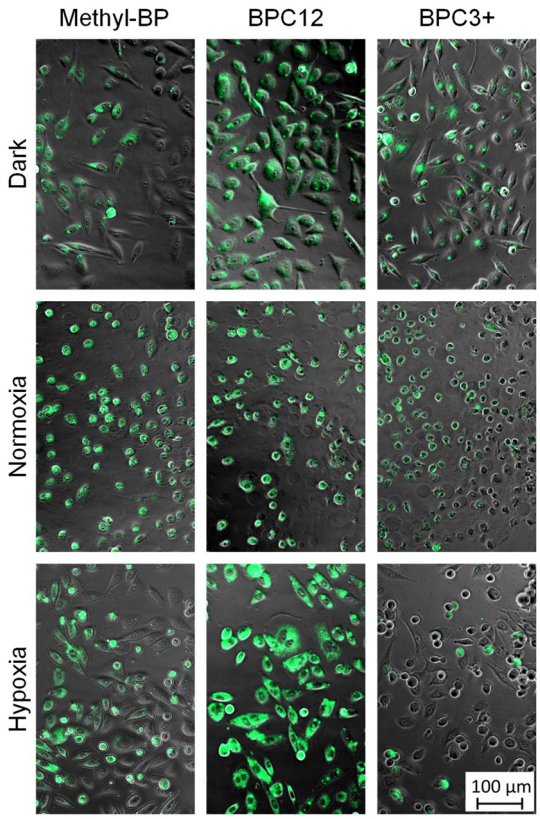

Fig. 2 Merged phase-contrast and fluorescence images of PC-3 cells treated with 6.0 µM of Methyl-BP, BPC12 and BPC3+ in the dark and after illumination with 53.5 J/cm^2 in both normoxic and hypoxic conditions. Between illumination and imaging cells were kept in the dark at + 37 °C and 5% CO_2 for 24 h

3.3.1 Phototoxicity in normoxic conditions

The merged phase-contrast and fluorescence images of the cells treated with 6.0 µM of the studied dyes without illumination (dark) and upon illumination with 53.5 J/cm^2 light dosage (27 mW/cm^2 for 33 min) in normoxic conditions are presented in Fig. 2 (top and middle rows). It is known that the Methyl-BP accumulates into lipid droplets [36, 37]. Kuimova et al. [12] have concluded that the BPC12 localizes into endocytic vesicles in human ovarian carcinoma cell line SK-OV-3 as a result of endocytic internalization. This explains the similar localization of BPC12 with the Methyl-BP observed in Fig. 2 (top row). The BPC3+ dye has more defined localization in the central part of the cell (Fig. 2, top row), adjacent but clearly distinct from the nucleus. This noticeably different BPC3+ cellular distribution compared with that for Methyl-BP or BPC12 has not been ever reported to the best of our knowledge. One

possible localization site is mitochondria, since lipophilic cations, e.g., BPC3+, easily penetrate the mitochondrial inner membrane due to the potential and pH gradient over the membrane [38–40]. To prove this, we performed co-localization studies for all three BODIPY derivatives with a mitochondrial marker (Supporting Information, Fig. S4). The obtained results agree with the literature reported above for Methyl-BP and BPC12 showing localization in granules or vesicles. The BPC3+ and Mitotracker have matching patterns, therefore, confirming the hypothesis of localization of the BPC3+ in the mitochondria.

Even though the Methyl-BP has the highest fluorescence quantum yield (Φ_{fl}, Table 1), its fluorescence intensity is rather weak after 24-h incubation (Fig. 2, top row), and only some cells have the dye accumulated inside. This might be explained by the long incubation time, during which the Methyl-BP may already be externalized from the cells. The fluorescence signals of both BPC12 and BPC3+ are more intense and seen in every cell (Fig. 2, top row). In addition, their fluorescence does not fade in 24 h, most likely due to the long carbon chains in their structure (Chart 1A) which helps to keep the dyes attached to the lipid structures longer.

Cells treated with 6.0 µM dye and illuminated with 53.5 J/cm^2 light dosage demonstrate a significant change in the cell morphology (Fig. 2, middle row) compared with the cells kept in the dark (Fig. 2, top row). A fluorescence signal is still seen inside the cells that have lost their original morphology with all the dyes (Fig. 2, middle row). In addition, the cells kept in the dark (Fig. 2, top row) retain their typical morphology as can be seen by comparing with 100% survival control in the absence of the dyes (Supporting Information, Fig. S5). This confirms that none of the studied dyes possesses any dark cytotoxicity. Thus, the observed changes in the morphology 24 h after the illuminations, such as swelling and rounding of the cells (Fig. 2, middle row), indicate a phototoxic effect for all the dyes [41]. Swelling can be a sign of necrosis [42] and reactive oxygen species are known to cause cell death by the pathway of necrosis [43]. We proved in the solution studies, that at least singlet oxygen is produced by all the studied BODIPY derivatives and can among others mediate the phototoxic effect. However, it should be pointed out that other reactive oxygen species may also contribute to the observed phototoxicity.

It should be noted that phototoxic effect may take time to develop, since the illumination may initially damage cell repair mechanisms and not cause straight fatality [44, 45]. Therefore, ATP levels were measured with viability assay only in 24 h after illuminations to ensure enough time for all possible mechanisms of cell death (i.e., apoptosis and/or necrosis [46]).

Dye concentration effect. Cell viabilities after treatment with different concentrations of the Methyl-BP, BPC12 and BPC3+ upon illumination with the light dosage of 53.5 J/cm^2 and in the dark are presented in Fig. 3. The results clearly show the dependence of the phototoxicity effect on the dye concentration. Both rotor molecules were studied at four concentrations. Due to the strong phototoxicity of Methyl-BP even at the lowest studied concentration, only two extreme concentrations were examined for this dye.

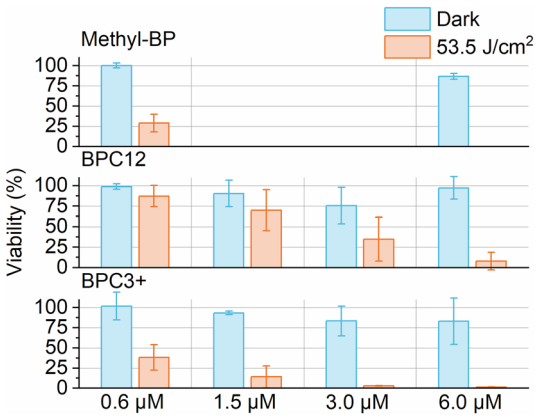

Fig. 3 Cell viabilities of PC-3 cells treated with 0.6 µM, 1.5 µM, 3.0 µM and 6.0 µM Methyl-BP, BPC12 and BPC3+ in the dark and after illumination with 53.5 J/cm^2. During illumination cells have been at + 37 °C and 5% CO_2. Error bars are 95% confidence intervals. Before performing viability assays cells were kept in the dark at + 37 °C and 5% CO_2 for 24 h

The increase of Methyl-BP concentration from 0.6 µM to 6.0 µM leads to the cell survival drop from 29.0% to a complete cell death after the illumination (Fig. 3) being in good agreement with the loss of typical morphology seen in Fig. 2 (middle row). The manufacturer of the Methyl-BP recommends to use 1–10 µM solutions for cell staining, and e.g., Nikon Microscopy U [47] generally suggests to use dyes in concentrations varying from nano- to micromolar. The chosen concentrations suite well to these recommendations.

The Methyl-BP and the BPC3+ rotor seem to be almost equally phototoxic at the lowest dye concentration (0.6 µM, Fig. 3) with the cell viabilities of 29.0% and 38.1%, respectively. The viability in the presence of the BPC3+ decreases from 38.1% to 1.2% with a tenfold concentration increase confirming the concentration dependency of the phototoxic effect.

While the BPC12 is almost non-toxic at its lowest concentration (Fig. 3), it still shows a significant cell viability drop upon the dye concentration increase. Although the difference between the 0.6 µM and 6.0 µM concentrations is notably high, the decrease of the viability (87.1% to 8.0%) is more gradual for the cells treated with the BPC12 compared with the BPC3+. The higher phototoxicity of BPC3+ rotor might be explained by its cellular localization if the dye targets mitochondria, consequently leading to mitochondrial autophagy and apoptosis [48]. Therefore, the BPC12

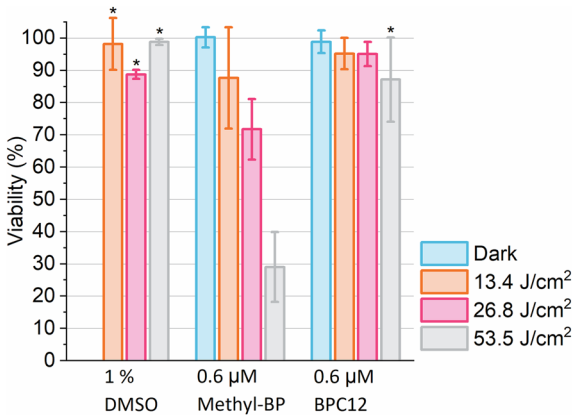

Fig. 4 Cell viabilities of PC-3 cells treated with 1% DMSO, 0.6 µM Methyl-BP and 0.6 µM BPC12 in the dark and after illumination with 3 different light doses: 13.4 J/cm^2, 26.8 J/cm^2 and 53.5 J/cm^2. During illumination, cells have been at + 37 °C and 5% CO_2. Error bars are 95% confidence intervals. Before performing viability assays cells were kept in the dark at + 37 °C and 5% CO_2 for 24 h. *P-value > 0.05, when compared to the dark control of the treatment

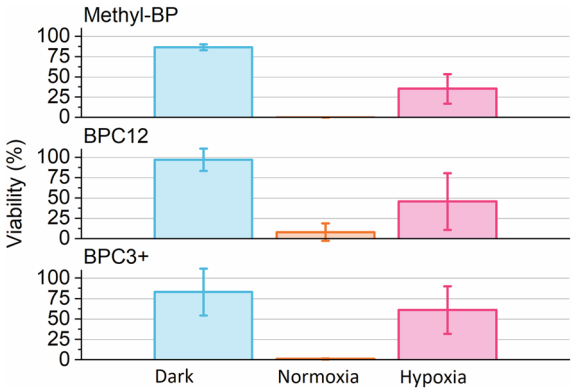

Fig. 5 Cell viabilities of PC-3 cells treated with 6.0 µM Methyl-BP, BPC12 and BPC3+ in the dark and after illumination with 53.5 J/cm^2 in both normoxic and hypoxic conditions. During illumination, cells have been at + 37 °C and 5% CO_2. Error bars are 95% confidence intervals. Before performing viability assays cells were kept in the dark at + 37 °C and 5% CO_2 for 24 h in normoxic condition

is clearly the best choice when working with higher than nanomolar concentrations.

Light dosage effect. By decreasing the light dose of the illumination, the light dose dependency of the phototoxic effect was studied for 0.6 µM Methyl-BP and BPC12. The dyes were chosen because of the largest difference in the measured cell viabilities between them at the chosen concentration after the highest light dose illumination (0.6 µM, Fig. 3). Cell viabilities in the dark and after illumination with different light dosages (13.4 J/cm^2, 26.8 J/cm^2 and 53.5 J/cm^2) for the Methyl-BP, BPC12 and 1% DMSO are presented in Fig. 4. The Methyl-BP demonstrates a slight phototoxicity already at the lowest illumination dose of 13.4 J/cm^2 and the phototoxic effect increases upon the raising of the illumination dose, showing a light dose dependent behavior. In contrast, the BPC12-treated cells show close to 100% survival at the light doses of 13.4 J/cm^2 of 26.8 J/cm^2.

At the highest light dose of 53.5 J/cm^2 (Fig. 4), the marginally decreased cell survival in the presence of BPC12 is not statistically different from the dark control cells treated with the BPC12, having a p-value of 0.34 (> 0.05 [49]). The viabilities for the cells free of any dye (1% DMSO) under different light dosages are close to 100% survival with p-values of 0.66, 0.31 and 0.93 at 13.4, 26.8 and 53.5 J/cm^2, respectively. This additionally confirms that the viability changes are caused by the phototoxicity of the studied dyes where applicable.

Most of the microscopy techniques operate with over 100 mW/cm^2 power densities [50]. This means only 9-min illumination time is needed to reach 53.5 J/cm^2 light dosage, which is already fatal when using 6.0 µM Methyl-BP as a dye. The lowest light dosage used in this study (13.4 J/cm^2) would be acquired with an illumination time of only 2 min with 100 mW/cm^2 power density. This should be carefully considered when using a dye with phototoxic properties for live-cell imaging, especially for long-term experiments.

3.3.2 Phototoxicity in hypoxic conditions

The oxygen sensitivity of the phototoxic effect was investigated by comparing the viabilities of the studied dyes in normoxic (20.95% of oxygen) and hypoxic (≈0.08% of oxygen) conditions. The viabilities of the 6.0 µM Methyl-BP-, BPC12−, and BPC3+-treated cells in normoxia and hypoxia after illumination with 53.5 J/cm^2 light dose and in normoxic dark are presented in Fig. 5. The highest dye concentration of 6.0 µM was chosen, as it caused almost complete cell death for all the studied dyes in normoxic conditions making it easier to see any cell viability improvement in hypoxic conditions.

The hypothesis of the study was that the phototoxic effect is caused by a singlet oxygen formation upon illumination, which could be inhibited by removing oxygen from the incubator. All the dyes show improved cell viability in lack of oxygen (Fig. 5): the Methyl-BP has an increase from 0.0 to 35.4%, the BPC12 from 8.0 to 45.8% and the BPC3+ from 1.2 to 61.0%, confirming that the phototoxicity is mainly mediated by reactive oxygen species. Similar oxygen-dependent behavior is also seen in fluorescence images (Fig. 2, bottom row). Even though some morphological changes are observed in hypoxia, the morphology of the cells resembles more the morphology seen in the dark controls than in normoxic conditions. The morphology changes are less pronounced for the

BPC12-treated cells than for the ones containing Methyl-BP or BPC3+.

The hypoxic (≈ 0.08% of oxygen) conditions noticeably improved the cell viabilities for all three BODIPY dyes, thus confirming the phototoxic effect being related to reactive oxygen species formation, e.g., singlet oxygen generation. This result agrees with the solution studies showing possibility of singlet oxygen generation in the presence of all studied dyes. However, the phototoxicity of the dyes in live cells differ and the largest one is observed for the non-rotor Methyl-BP dye.

Generally, the dyes with high fluorescence quantum yields demonstrate lower phototoxicity because the domination of fluorescence decreases the possibility of triplet state formation. Thus, the relatively low amount of singlet oxygen (3–15% according to our data and up to 21–29% reported in literature [17]) in the presence of non-rotor Methyl-BP dye does not cause any immediate fatal phototoxicity in short-term imaging which is in agreement with the dye manufacturer's information. However, our data shows that the small damages caused by tiny amounts of singlet oxygen are accumulated in cells in time and upon multiple illuminations in long-term imaging, and finally result in significant phototoxicity and cell death. Thus, it appears that even this quite low amount of triplet states of the non-rotor dye has a larger effect than that of the rotor dyes. Although the rotor dyes have lower fluorescence quantum yields, allowing the excitation energy to release via other paths, the ISC^S does not seem to be favored. Indeed, the rotor dyes demonstrate lower singlet oxygen formation in solutions and milder phototoxicity in cells upon illumination compared to the non-rotor dye. It speaks to the conclusion that in case of rotor dyes ISC^S is almost not realized due to efficient IMR and subsequent fast IC.

Furthermore, while the possibility for the IMR reduces the phototoxicity of a dye, other structural properties of the imaging probes are also important. Thus, it turns out that a positive charge of a dye may neglect the benefit of the IMR as in the case of BPC3+ when the singlet oxygen formation is highly dependent on the environmental polarity. The positive charge of the rotor seems to determine the specific cellular targeting to mitochondria that may also result in the increase of the phototoxic effect. As a final point, the viability studies clearly show that the BPC12 is the safest lipid-probe among the studied ones and can be used even at relatively high concentration (6.0 μM) and light dose (53.5. J/cm^2).

4 Conclusions

Both the solution and the cell studies led to the conclusion that Methyl-BP and positively charged BPC3+ generate higher concentrations of singlet oxygen and consequently cause the stronger phototoxicity than the BPC12. Thus, due to their phototoxicity, Methyl-BP and BPC3+ can only be used for short-term imaging experiments. However, the BPC12 and probably other neutral BODIPY-based molecular rotors with IMR should be substantially more suitable for long-term or high-light-dose live-cell imaging experiments. As an extra advantage, they possess moderate fluorescence quantum yields and offer multifaceted environment-sensing properties. To conclude, the results presented in this manuscript should be considered when performing long-lasting, high-light-dose, demanding live-cell fluorescence imaging experiments to avoid any misleading results.

Supplementary Information The online version contains supplementary material available at https://doi.org/10.1007/s43630-022-00250-y.

Acknowledgements BPC3+ rotor was kindly provided by Dr. Marina Kuimova (Imperial College London). We thank the DDCB core facility supported by the University of Helsinki (HiLIFE) and Biocenter Finland.

Author contributions Conceptualization: IK, ND and EL; data curation: IK; formal analysis: IK; funding acquisition: TL, EV-L and EL; investigation: IK, ND, PI, EV-L and EL; methodology: IK, ND and EL; project administration: EL; resources: AE; supervision: EL, TL and EV-L; validation: IK, ND, PI, TL, EV-L and EL; visualization: IK; writing—original draft: IK; writing—review and editing: IK, ND, PI, AE, TL, EV-L and EL.

Funding The study was funded by Academy of Finland (316893, Timo Laaksonen; 311362, Elina Vuorimaa-Laukkanen & 323669, Ekaterina Lisitsyna).

Declarations

Conflict of interests The authors declare that they have no competing interests.

References

1. Karolin, J., Johansson, L. B. A., Strandberg, L., & Ny, T. (1994). Fluorescence and absorption spectroscopic properties of dipyrromethene boron difluoride (BODIPY) derivatives in liquids, lipid membranes, and proteins. *Journal of the American Chemical Society, 116*(17), 7801–7806. https://doi.org/10.1021/ja00096a042
2. Haidekker, M. A., & Theodorakis, E. A. (2010). Environment-sensitive behavior of fluorescent molecular rotors. *Journal of Biological Engineering, 4*(11), 14. https://doi.org/10.1186/1754-1611-4-11
3. Zhong, C. (2015). The driving forces for twisted or planar intramolecular charge transfer. *Physical Chemistry Chemical Physics: PCCP, 17*(14), 9248–9257. https://doi.org/10.1039/C4CP02381A
4. Kee, H. L., Kirmaier, C., Yu, L., Thamyongkit, P., Youngblood, W. J., Calder, M. E., Ramos, L., Noll, B. C., Bocian, D. F., Scheidt, W. R., Birge, R. R., Lindsey, J. S., & Holten, D. (2005). Structural control of the photodynamics of boron−dipyrrin complexes. *The Journal of Physical Chemistry B, 109*(43), 20433–20443. https://doi.org/10.1021/jp0525078
5. Prlj, A., Vannay, L., & Corminboeuf, C. (2017). Fluorescence quenching in BODIPY dyes: The role of intramolecular interactions and charge transfer. *Helvetica Chimica Acta, 100*(6), e1700093. https://doi.org/10.1002/hlca.201700093
6. Polita, A., Toliautas, S., Žvirblis, R., & Vyšniauskas, A. (2020). The effect of solvent polarity and macromolecular crowding on the viscosity sensitivity of a molecular rotor BODIPY-C10. *Physical Chemistry Chemical Physics: PCCP, 22*(16), 8296–8303. https://doi.org/10.1039/C9CP06865A
7. Haidekker, M. A., Nipper, M., Mustafic, A., Lichlyter, D., Dakanali, M., & Theodorakis, E. A. (2010). Dyes with Segmental Mobility: Molecular Rotors. In A. P. Demchenko (Ed.), *Advanced fluorescence reporters in chemistry and biology I. Springer Series on Fluorescence (Methods and Applications)* (8th ed., pp. 267–308). Springer. https://doi.org/10.1007/978-3-642-04702-2_8.
8. Ogle, M. M., Smith McWilliams, A. D., Ware, M. J., Curley, S. A., Corr, S. J., & Martí, A. A. (2019). Sensing temperature in vitro and in cells using a BODIPY molecular probe. *The Journal of Physical Chemistry B, 123*(34), 7282–7289. https://doi.org/10.1021/acs.jpcb.9b04384
9. Kuimova, M. K. (2012). Mapping viscosity in cells using molecular rotors. *Physical Chemistry Chemical Physics, 14*(37), 12671–12686. https://doi.org/10.1039/c2cp41674c
10. Su, D., Teoh, C. L., Gao, N., Xu, Q.-H., & Chang, Y.-T. (2016). A simple BODIPY-based viscosity probe for imaging of cellular viscosity in live cells. *Sensors, 16*(9), 9. https://doi.org/10.3390/s16091397
11. Vyšniauskas, A., López-Duarte, I., Duchemin, N., Vu, T.-T.T., Wu, Y., Budynina, E. M., Volkova, Y. A., Peña Cabrera, E., Ramírez-Ornelas, D. E., & Kuimova, M. K. (2017). Exploring viscosity, polarity and temperature sensitivity of BODIPY-based molecular rotors. *Physical Chemistry Chemical Physics: PCCP, 19*(37), 25252–25259. https://doi.org/10.1039/C7CP03571C
12. Kuimova, M. K., Yahioglu, G., Levitt, J. A., & Suhling, K. (2008). Molecular rotor measures viscosity of live cells via fluorescence lifetime imaging. *Journal of the American Chemical Society, 130*(21), 6672–6673. https://doi.org/10.1021/ja800570d
13. Lisitsyna, E., Efimov, A., Depresle, C., Cauchois, P., Vuorimaa-Laukkanen, E., Laaksonen, T., & Durandin, N. (2021). Deciphering multiple critical parameters of polymeric self-assembly by fluorescence spectroscopy of a single molecular rotor BODIPY-C12. *Macromolecules, 54*(2), 655–664. https://doi.org/10.1021/acs.macromol.0c02167
14. Ashokkumar, P., Ashoka, A. H., Collot, M., Das, A., & Klymchenko, A. S. (2019). A fluorogenic BODIPY molecular rotor as an apoptosis marker. *Chemical Communications, 55*(48), 6902–6905. https://doi.org/10.1039/C9CC03242H
15. Priessner, M., Summers, P. A., Lewis, B. W., Sastre, M., Ying, L., Kuimova, M. K., & Vilar, R. (2021). Selective detection of Cu + ions in live cells via fluorescence lifetime imaging microscopy. *Angewandte Chemie International Edition, 60*, 7. https://doi.org/10.1002/anie.202109349
16. Robson, J. A., Kubánková, M., Bond, T., Hendley, R. A., White, A. J. P., Kuimova, M. K., & Wilton-Ely, J. D. E. T. (2020). Simultaneous detection of carbon monoxide and viscosity changes in cells. *Angewandte Chemie International Edition, 59*(48), 21431–21435. https://doi.org/10.1002/anie.202008224
17. Zhang, X., & Zhu, J. (2019). BODIPY parent compound: Excited triplet state and singlet oxygen formation exhibit strong molecular oxygen enhancing effect. *Journal of Luminescence, 212*, 286–292. https://doi.org/10.1016/j.jlumin.2019.04.050
18. Briviba, K., Klotz, L. O., & Sies, H. (1997). Toxic and signaling effects of photochemically or chemically generated singlet oxygen in biological systems. *Biological Chemistry*, *378*(11), 1259–1265. http://europepmc.org/abstract/MED/9426185.
19. Saari, H., Lisitsyna, E., Rautaniemi, K., Rojalin, T., Niemi, L., Nivaro, O., Laaksonen, T., Yliperttula, M., & Vuorimaa-Laukkanen, E. (2018). FLIM reveals alternative EV-mediated cellular up-take pathways of paclitaxel. *Journal of Controlled Release, 284*, 133–143. https://doi.org/10.1016/j.jconrel.2018.06.015
20. Squirrell, J. M., Wokosin, D. L., White, J. G., & Bavister, B. D. (1999). Long-term two-photon fluorescence imaging of mammalian embryos without compromising viability. *Nature Biotechnology, 17*(8), 763–767. https://doi.org/10.1038/11698
21. Tosheva, K. L., Yuan, Y., Matos Pereira, P., Culley, S., & Henriques, R. (2020). Between life and death: Strategies to reduce phototoxicity in super-resolution microscopy. *Journal of Physics D: Applied Physics, 53*(16), 163001. https://doi.org/10.1088/1361-6463/ab6b95
22. Levitt, J. A., Kuimova, M. K., Yahioglu, G., Chung, P., Suhling, K., & Phillips, D. (2009). Membrane-bound molecular rotors measure viscosity in live cells via fluorescence lifetime imaging. *The Journal of Physical Chemistry C, 113*(27), 11634–11642. https://doi.org/10.1021/jp9013493
23. Sherin, P. S., López-Duarte, I., Dent, M. R., Kubánková, M., Vyšniauskas, A., Bull, J. A., Reshetnikova, E. S., Klymchenko, A. S., Tsentalovich, Y. P., & Kuimova, M. K. (2017). Visualising the membrane viscosity of porcine eye lens cells using molecular rotors. *Chemical Science, 8*, 3523–3528. https://doi.org/10.1039/C6SC05369F
24. Spangenburg, E. E., Pratt, S. J. P., Wohlers, L. M., & Lovering, R. M. (2011). Use of BODIPY (493/503) to visualize intramuscular lipid droplets in skeletal muscle. *BioMed Research International, 2011*(598358), 8. https://doi.org/10.1155/2011/598358
25. Walther, T. C., & Farese, R. V. (2012). Lipid droplets and cellular lipid metabolism. *Annual Review of Biochemistry, 81*(1), 687–714. https://doi.org/10.1146/annurev-biochem-061009-102430
26. Wagner, R. W., & Lindsey, J. S. (1996). Boron-dipyrromethene dyes for incorporation in synthetic multi-pigment light-harvesting arrays. *Pure and Applied Chemistry, 68*(7), 1373–1380. https://doi.org/10.1351/pac199668071373
27. Durán-Sampedro, G., Agarrabeitia, A. R., Cerdán, L., Pérez-Ojeda, M. E., Costela, A., García-Moreno, I., Esnal, I., Bañuelos, J., Arbeloa, I. L., & Ortiz, M. J. (2013). Carboxylates versus fluorines: Boosting the emission properties of commercial BODIPYs in liquid and solid media. *Advanced Functional Materials, 23*, 4195–4205. https://doi.org/10.1002/adfm.201300198
28. Promega Corporation. (2015). CellTiter-Glo ® Luminescent cell viability assay cell viability assay, p. 14.

29. Reichardt, C., & Welton, T. (2010). Appendix A. Properties, Purification, and use of organic solvents. In C. Reichardt & T. Welton (Eds.), *Solvents and solvent effects in organic chemistry* (pp. 549–586). Wiley, Hoboken. https://doi.org/10.1002/9783527632220.app1.
30. Valeur, B., & Berberan-Santos, M. N. (2013). *Molecular fluorescence: Principles and applications* (2nd ed.). Hoboken: Wiley-VCH.
31. Wang, L., Bai, J., & Qian, Y. (2019). Synthesis of a triphenylamine BODIPY photosensitizer with D-A configuration and its application in intracellular simulated photodynamic therapy. *New Journal of Chemistry, 43*, 16829–16834. https://doi.org/10.1039/C9NJ04166D
32. Filatov, M. A., Karuthedath, S., Polestshuk, P. M., Callaghan, S., Flanagan, K. J., Telitchko, M., Wiesner, T., Laquai, F., & Senge, M. O. (2018). Control of triplet state generation in heavy atom-free BODIPY–anthracene dyads by media polarity and structural factors. *Physical Chemistry Chemical Physics: PCCP, 20*, 8016–8031. https://doi.org/10.1039/C7CP08472B
33. Wang, Z., Ivanov, M., Gao, Y., Bussotti, L., Foggi, P., Zhang, H., Russo, N., Dick, B., Zhao, J., Di Donato, M., Mazzone, G., Luo, L., & Fedin, M. (2020). Spin-orbit charge-transfer intersystem crossing (ISC) in compact electron donor-acceptor Dyads: ISC mechanism and application as novel and potent photodynamic therapy reagents. *Chemistry A European Journal, 26*, 1091–1102. https://doi.org/10.1002/chem.201904306
34. Battino, R., Rettich, T. R., & Tominaga, T. (1983). The solubility of oxygen and ozone in liquids. *Journal of Physical and Chemical Reference Data, 12*, 163–178. https://doi.org/10.1063/1.555680
35. Lutkus, L. V., Rickenbach, S. S., & McCormick, T. M. (2019). Singlet oxygen quantum yields determined by oxygen consumption. *Journal of Photochemistry and Photobiology A: Chemistry, 378*, 131–135. https://doi.org/10.1016/j.jphotochem.2019.04.029
36. Listenberger, L. L., Ostermeyer-Fay, A. G., Goldberg, E. B., Brown, W. J., & Brown, D. A. (2007). Adipocyte differentiation-related protein reduces the lipid droplet association of adipose triglyceride lipase and slows triacylglycerol turnover. *Journal of Lipid Research, 48*(12), 2751–2761. https://doi.org/10.1194/jlr.M700359-JLR200
37. Horn, P. J., James, C. N., Gidda, S. K., Kilaru, A., Dyer, J. M., Mullen, R. T., Ohlrogge, J. B., & Chapman, K. D. (2013). Identification of a new class of lipid droplet-associated proteins in plants. *Plant Physiology, 162*(4), 1926–1936. https://doi.org/10.1104/pp.113.222455
38. Liberman, E. A., Topaly, V. P., Tsofina, L. M., Jasaittis, A. A., & Skulachev, V. P. (1969). Mechanism of coupling of oxidative phosphorylation and the membrane potential of mitochondria. *Nature, 222*(5198), 1076–1078. https://doi.org/10.1038/222107 6a0
39. Azzone, G.F., Pietrobon, D., & Zoratti, M. (1984). Determination of the proton electrochemical gradient across biological membranes. In C.P. Lee (Ed.) (Vol. 13, pp. 1–77). Elsevier. https://doi.org/10.1016/B978-0-12-152513-2.50008-8.
40. Ross, M. F., Kelso, G. F., Blaikie, F. H., James, A. M., Cochemé, H. M., Filipovska, A., Da Ros, T., Hurd, T. R., Smith, R. A. J., & Murphy, M. P. (2005). Lipophilic triphenylphosphonium cations as tools in mitochondrial bioenergetics and free radical biology. *Biochemistry (Moscow), 70*(2), 222–230. https://doi.org/10.1007/s10541-005-0104-5
41. Laissue, P. P., Alghamdi, R. A., Tomancak, P., Reynaud, E. G., & Shroff, H. (2017). Assessing phototoxicity in live fluorescence imaging. *Nature Methods, 14*, 657–661. https://doi.org/10.1038/nmeth.4344
42. Yang, Y., Jiang, G., Zhang, P., & Fan, J. (2015). Programmed cell death and its role in inflammation. *Military Medical Research, 2*(12), 12. https://doi.org/10.1186/s40779-015-0039-0
43. Wiman, K. G., & Zhivotovsky, B. (2017). Understanding cell cycle and cell death regulation provides novel weapons against human diseases. *Journal of Internal Medicine, 281*(5), 483–495. https://doi.org/10.1111/joim.12609
44. Wäldchen, S., Lehmann, J., Klein, T., van de Linde, S., & Sauer, M. (2015). Light-induced cell damage in live-cell super-resolution microscopy. *Scientific Reports, 5*(1), 15348. https://doi.org/10.1038/srep15348
45. Maier, K., Schmitt-Landgraf, R., & Siegemund, B. (1991). Development of an in vitro test system with human skin cells for evaluation of phototoxicity. *Toxicology in Vitro, 5*(5), 457–461. https://doi.org/10.1016/0887-2333(91)90072-L
46. Cell Viability GuidelHow to Measure Cell Viability. (2021). https://fi.promega.com/resources/guides/cell-biology/cell-viability/#references-43c84328-610b-4941-a445-69485b126328. Accessed 4 Oct 2021.
47. Spring, K. R., & Davidson, M. W. (2021). *Introduction to Fluorescence Microscopy*. Nikon Instruments Inc. https://www.microscopyu.com/techniques/fluorescence/introduction-to-fluorescence-microscopy.
48. Zhao, J., Zou, M., Huang, M., Zhang, L., Yang, K., Zhao, S., & Liu, Y.-M. (2020). A multifunctional nanoprobe for targeting tumors and mitochondria with singlet oxygen generation and monitoring mitochondrion pH changes in cancer cells by ratiometric fluorescence imaging. *Chemical Science, 11*(14), 3636–3643. https://doi.org/10.1039/D0SC00757A
49. Kim, T. K. (2015). T test as a parametric statistic. *Korean Journal of Anesthesiology, 68*(6), 540–546. https://doi.org/10.4097/kjae.2015.68.6.540
50. Schneckenburger, H., Weber, P., Wagner, M., Bruns, T., Richter, V., Schickinger, S., & Wittig, R. (2012). Multidimensional fluorescence microscopy in live cell imaging—a mini review. *Photonics & Lasers in Medicine, 1*(1), 35–40. https://doi.org/10.1515/plm-2011-0011